PII: S0955-2219(98)00151-4

0955-2219/98/$—see front matter

Mechanical Characterization of Al_2O_3/ZrO_2 Hybrid Laminates

Peter Z. Cai, David J. Green* and Gary L. Messing

Department of Materials Science and Engineering The Pennsylvania State University, University Park, PA 16801, USA

(Received 1 September 1997; revised version received 10 May 1998; accepted 16 June 1998)

Abstract

Significant residual stresses due to the thermal expansion mismatch were found in the Al_2O_3/Ce–ZrO_2 laminated composites investigated in this study. The residual stresses were measured by evaluating the difference in indentation crack length, with and without the residual stresses. The obtained residual stress values are in good agreement with the calculated residual stresses from the measured coefficients of thermal expansion and elastic constants. The laminated structure was found to give rise to an increase in indentation strength compared to monolithic alumina. This apparent increase in fracture toughness can be explained as the effect of the compressive residual stress in the outer Al_2O_3 layer and can be controlled by changing the relative layer thickness. For the size scale studied here, the zirconia-based layers did not appear to play a major role in the final failure process. © *1998 Elsevier Science Limited. All rights reserved*

1 Introduction

Laminated ceramic composites, which are composed of alternating layers of two or more different ceramic materials or phases, have emerged during the past several years as a viable alternative to the more widely studied fiber-reinforced ceramic composites. Although laminated ceramic composites have not been extensively investigated, they have shown a promising future from the limited work reported in this field. Fabrication of these laminated structures usually employs relatively low-cost conventional processing routes, such as tape casting, sequential slip casting and coating techniques. For the majority of these composites, optimization of fracture behavior is not contingent upon a low fracture energy interface, as often required in fiber reinforced ceramic composites. Hence laminated ceramic composites hold the promise to overcome some of the key problems that are associated with fiber reinforced composites, namely, low transverse strength and high processing cost.

An example of a ceramic laminate with strong interfaces was demonstrated by Marshall, *et al.*[1] Laminates with layers of Ce–ZrO_2 and either Al_2O_3 or Al_2O_3/Ce–ZrO_2 mixture were formed by sequential centrifuging of colloidal dispersions containing the suspended particles. It was found that the presence of the Al_2O_3-containing layers truncated the elongated transformation zone of Ce–ZrO_2, and, somewhat unexpectedly, led to increased widths of the transformation zone near the Al_2O_3 interface. The combined effect of the zone spreading perpendicular to the direction of crack propagation and the truncation of the frontal transformation zone caused the fracture toughness to increase from about 5 MPa $m^{1/2}$ to about 17 MPa $m^{1/2}$ for the layered material. Zone spreading and the toughening effects were also observed for specimens loaded in the orientation for cracks growing parallel to the layers.

Since any two materials almost always have different thermal expansion coefficients, incorporation of two dissimilar materials into a composite invariably introduces residual stresses. Residual stresses were observed in Al_2O_3–ZrO_2 trilayers and multilayers.[2–5] It was shown[2] that the presence of compressive residual stresses on the surface gives rise to higher values of strength and post-indentation strength over the monolithic counterparts. If the compressive residual stresses are viewed as contributing to the toughness of the outer layer,[6] the deliberate introduction of residual stresses in the laminated composites enhances the resistance to crack extension, and the laminates may exhibit a rising toughness curve, i.e. R-curve behavior.

*To whom correspondence should be addressed.

This paper examines the effect of the residual compressive stress in the outer Al_2O_3 layer of a tape-cast laminated composite consisting of alternating layers of Al_2O_3 and a Ce–ZrO_2/Al_2O_3 mixture. The residual stresses were estimated by contrasting the indentation crack size on the Al_2O_3 surface of the composite with the indentation crack size on the monolithic Al_2O_3. The experimental results are compared with the analytical results calculated from the coefficients of thermal expansion. Strength tests were performed on both the hybrid laminates and 'laminates' of a single composition, i.e. the latter consisting solely of one layer constituent. Flexural strength tests were also conducted on indented samples, and the initial indentation crack shape as well as the amount of stable growth prior to failure were determined by optical and electron microscopy. The effect of the residual stress on the indentation strength behavior is demonstrated and the effect of laminate geometry on the final failure instability is discussed.

2 Experimental

The Al_2O_3 and Ce–ZrO_2/Al_2O_3 hybrid laminates were fabricated by tape casting and lamination, as detailed in Refs. 7 and 8. Addition of Al_2O_3 in the ZrO_2 layers was used to eliminate the processing defects associated with mismatch in sintering shrinkage and thermal expansion between the layers. Tapes consisting of MgO-doped Al_2O_3 (Premalox, Alcoa), and a mixture of 70 wt% CeO_2-stabilized ZrO_2 (TZ-12Ce, Tosoh) and 30 wt% Al_2O_3, were prepared. The laminates were formed by thermal lamination (90°C, 48 MPa) of stacked tapes, followed by binder burnout (450°C for 8 h) and pressureless sintering of the green laminates (5°C min^{-1} to 1530°C for 90 min).

Three types of laminates were processed with different layer thicknesses and layer volume fractions. The first type, 1A–1Z, has alternating A100 and Z70–A30 layers of 120–150 μm thickness, with both surface layers being A100. The second type, 1A–2Z, has two Z70–A30 layers for each Al_2O_3 layer, with the surface layers also being A100. The third type, 0·5A—0·5Z, has the same layer sequence as the first type, but with approximately half of the layer thicknesses. The smaller layer thickness in 0·5A–0·5Z was achieved during the lamination process by applying a pressure (about 60 MPa) to the stacked green tapes which filled about half of the area of the lamination die. The lateral expansion of the stacked green tapes caused by the pressure filled the die, thereby decreasing the layer thickness by approximately half (60~80 μm). In addition to the three types of composite laminates, monocomposition laminates comprising solely of A100 or Z70–A30 were also processed under similar conditions. Most of the samples had a total of 22 to 23 layers. The laminated green samples were machined into bend bars, and most of the as-sintered bend bars had nominal dimensions of 3×3×26 mm. Some of the samples had somewhat smaller thicknesses (2 mm).

The strength of the as-processed laminates was measured in four-point flexure with an inner span of 9·8 mm and an outer span of 22·2 mm. The specimen was oriented so that the tensile stress was parallel to the layers. A displacement rate of 1 mm min^{-1} was used, and the samples failed within 10 s of loading. Post-indentation strengths were determined in the same flexural loading configuration with a Vickers indent placed in the center of the tensile surface of the specimen. Indentation forces of 19·6, 49, 98 and 196 N were used. An average of four samples were tested for each indentation force and for as-processed strength measurements. Following the fracture of the specimen, the tensile surface was examined to check if the failure initiated from the indent. For some of the indentation-strength specimens, multiple (about 10) indents were evenly placed between the inner span to determine the extent of stable indentation crack growth during flexure.

Both the cross-section and the A100 surface of some sintered laminates were polished to 1 μm surface finish for indentation studies. Vickers indents with indentation forces of 19·6, 49, 98 and 196 N were generated on the polished A100 surfaces of the composite laminates and the monocomposition laminates. Four to five indents were made for each load. The indent diagonals were measured using the optical microscope that was attached to the indenter (Leco V-100-C1 Hardness Tester), whereas the indentation crack lengths were measured using another microscope (Nikon Epiphot or Olympus BX60MF) for which the light beam area could be adjusted. To convincingly determine the crack tip position for each indentation crack, the light beam was reduced so that the crack tip was in the dark field immediately next to the beam area. This technique gives a clear definition of the crack path. The surface traces of the indentation crack after the flexural failure in the multiple indent samples were also determined using this technique. In addition, Vickers indents were generated at indentation forces of 9·8 or 19·6 N in various positions on the polished cross-sections of the hybrid laminates.

The fracture surfaces of the strength and indentation strength specimens were examined by a scanning electron microscope (SEM, ISI ABT SX40A) and a stereoscope (Nikon AFX-IIA) to

determine the flaw origin and the final flaw size. The depth of the indentation crack was measured on the fracture surface using the same beam-narrowing technique.

The elastic modulus of the monocomposition laminates was determined by the sound velocity technique (Ultran Pulse Receiver HF-400; Ultran WC25-10 Transducer). The technique involves vibrating piezoelectric crystals at a set frequency and determining the transit time for a longitudinal sound wave to travel across the specimen. The velocity of the longitudinal wave, v, is related to the Young's modulus, E, as

$$v = \sqrt{\frac{E(1-\nu)}{\rho(1+\nu)(1-2\nu)}} \tag{1}$$

where the Poisson's ratio, ν, was assumed to be 0·24.

3 Results and discussion

3.1 Modulus, hardness and toughness of monocomposition laminates

The Young's moduli measured by the sound velocity technique were approximately 400 and 265 GPa for A100 and Z70–A30, respectively. The modulus of a typical Ce-stabilized ZrO_2 being 200 GPa, the measured modulus for Z70–A30 agrees well with the Voigt–Reuss average (264 GPa). The hardness of the monocomposition laminates, H, was calculated from the length of the half indent diagonal, a, by the following relationship:

$$H = 0{\cdot}47\frac{P}{a^2} \tag{2}$$

where P is the indentation force. The toughness, K_{Ic}, for the two materials was calculated from the as-indented crack length, c_0, by[9,10]

$$K_{Ic} = \chi\frac{P}{c_0^{3/2}} \tag{3}$$

where χ is a constant related to the magnitude of the residual stress field associated with the indentation. For many ceramics, the constant χ is approximated as $0{\cdot}016\sqrt{E/H}$ where E is the Young's modulus of the material.[9] The calculated hardness and toughness values are tabulated in Table 1. Note the Z70–A30 toughness values are absent for indentation forces of 19·6, 49 N, because the Vickers indentation at such load levels did not produce radial cracks at the corners of the indent.

3.2 Residual stress measurements

Since the coefficient of thermal expansion of Al_2O_3 layers is smaller than that of the Z70–A30, the A100 surface layers are expected to be in biaxial compression. The surface compression leads to a decrease in indentation crack length compared to the monolithic Al_2O_3. The magnitude of the compressive stress in turn can be estimated from the difference in indentation crack length between a residually stressed surface and a stress-free surface.[2,11–15] In the absence of the residual stress, the indentation crack length, c_0, is determined by the critical stress intensity factor, K_{Ic}, as expressed in eqn (3). In the presence of a uniform residual stress field, σ_r, the stress intensity factor becomes

$$K_{Ic} = \chi\frac{P}{c_1^{3/2}} + \Phi\sigma_r\sqrt{c_1} \tag{4}$$

where c_1 is the indentation crack length in the presence of the residual stress field, and Φ is a constant related to crack geometry and loading condition. Equating eqns (3) and (4) yields

$$\frac{P}{c_0^{3/2}} - \frac{P}{c_1^{3/2}} = \frac{\Phi}{\chi}\sigma_r\sqrt{c_1} \tag{5}$$

Therefore, if we plot the left-hand side of eqn (5) versus $\frac{\Phi}{\chi}\sqrt{c_1}$, the slope will be σ_r. The constant Φ is equal to $1{\cdot}12\,\frac{2}{\sqrt{\pi}} = 1{\cdot}26$ for a semicircular surface crack. The residual stress can also be calculated for each indentation force by solving for σ_r from eqns (3) and (4), which yields

Table 1. Measured Young's modulus using the sound velocity technique and calculated hardness and toughness from Vickers indentation for A100 and Z70–A30

	A100 (100% Al_2O_3)			*Z70–A30 (70 wt% Ce–ZrO_2/30 wt% Al_2O_3)*		
Indentation load (N)	H *(GPa)*	K_{Ic} *(MPa–$m^{0.5}$)*	E *(GPa)*	H *(GPa)*	K_{Ic} *(MPa $m^{0.5}$)*	E *(GPa)*
19·6	14·8 ± 0·4	3·8 ± 0·6				
49	15·1 ± 0·2	3·2 ± 0·4		12·2 ± 0·7		
98	15·0 ± 0·3	3·1 ± 0·3		12·3 ± 0·4	8·6 ± 1·2	
196	14·9 ± 0·4	3·3 ± 0·4		11·5 ± 0·2	7·2 ± 0·3	
Mean	14·9 ± 0·4	3·4 ± 0·5	400	12·0 ± 0·6	7·7 ± 1·0	265

$$\sigma_r = K_{Ic}\frac{1-(c_0/c_1)^{3/2}}{\Phi\sqrt{c_1}} \qquad (6)$$

where K_{Ic} can be determined from eqn (3). Therefore, by measuring the indentation crack lengths without and with the residual stress, the magnitude of the residual stress can be determined from the slope of a curve, as in eqn (5), or directly calculated from eqn (6). Figure 1 shows the measured indentation crack lengths on the A100 monocomposition laminate and on the A100 surface of the hybrid laminates. The indentation crack lengths for all the composites are smaller than the indentation cracks lengths on the monolithic A100 for a given indentation force, indicating that the A100 surface layer in the composites is in residual compression. This is consistent with the knowledge that A100 has a smaller coefficient of thermal expansion than Z70–A30.

The calculated residual stress from eqn (6) is shown in Fig. 2(a) for the three composites at various indentation forces. The magnitude of the calculated values at higher indentation forces tend to be smaller than the values at low indentation forces. This can be attributed to the fact that at high indentation forces the indentation crack may have penetrated the second layer, which is under biaxial tension. Since 0·5A–0·5Z has the smallest A100 surface layer thickness, the deviation of the calculated value at high indentation forces is more pronounced than in the case of 1A–1Z and 1A–2Z laminates. Figure 2(b) is a plot of $P(c_0^{-3/2} - c_1^{-3/2})$ as a function of $\frac{\Phi}{\chi}\sqrt{c_1}$, from which the more statistically accurate residual stress value is determined. The data for 1A–1Z and 1A–2Z at 196 N, as well as the data for 0·5A–0·5Z at 98 N and 196 N are not included, for the reason that the indentation cracks produced by these loads may

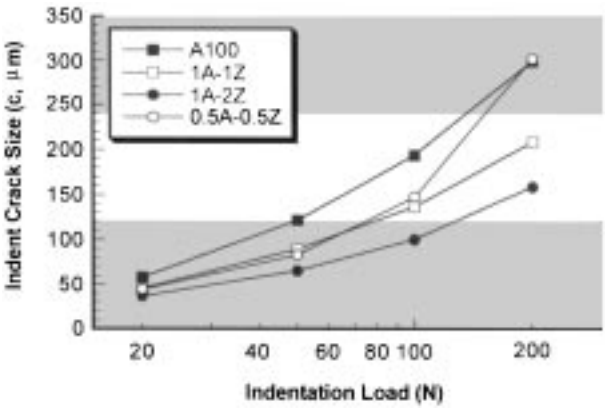

Fig. 1. Indentation crack size for monocomposition laminate A100 and hybrid laminates 1A–1Z, 1A–2Z and 0·5A0–0·5Z. The indents were placed on the Al_2O_3 surface of the laminates. Indentation forces used were 19·6, 49, 98 and 196 N. Shaded areas indicate a typical layer thickness.

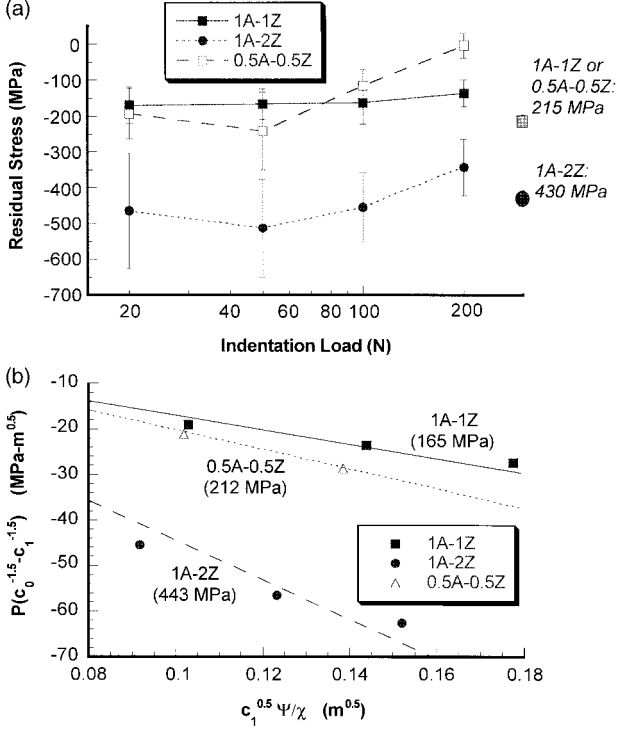

Fig. 2. (a) Calculated residual stress in the A100 surface layer using eqn (5) for 1A–1Z, 1A–2Z and 0·5A–0·5Z. The data points on the right represent the calculated values from the measured coefficients of thermal expansion. (b) Plot of $P(c_0^{-1.5} - c_1^{-1.5})$ as a function of $\Phi\sqrt{c_1}/\chi$. For clarity, only the average values are shown for each indentation force. The slope yields the value of the residual stress.

have entered the second layer. For clarity, only the average values at each indentation force are shown for each laminate. It can be seen that the magnitude of the residual stress for 1A–2Z is larger than that for 1A–1Z, and the residual stress in 1A–1Z is about the same as 0·5A–0·5Z. This is consistent with the elastic laminate stress analysis that the biaxial residual stress in a laminate is affected only by the relative thickness ratios between the layers. The residual stress results in Fig. 2 also show reasonable agreement with the calculated residual stresses from the measured coefficients of thermal expansion for both layers based on a viscoelastic stress analysis presented in Ref. 14. These calculated values are included in Fig. 2(a) for comparison.

The presence of residual stress was also demonstrated by the indentation cracks placed on the cross-section of the laminates. Figure 3 show an SEM micrograph of a 19·6 N indent in the A100 layer and an optical micrograph of a 49 N indent in the Z70–A30 layer. For the indent in the A100 layer, the set of indentation cracks perpendicular to the layer thickness direction was suppressed, suggesting the presence of the biaxial compressive stress within the layer. In contrast, the cracks in the layer direction grew extensively in response to the tensile edge-effect stress in the thickness direction. The indentation cracks within the Z70–A30 layer

showed opposite behavior, suggesting the presence of biaxial residual tension in the layer. In some of the indentation strength samples, the crack path also evidenced the presence of residual stress. As seen in Fig. 4, the crack tends to be deflected into the layer direction within the A100 layers due to the in-plane compressive stress. Similar tortuous crack paths were also observed in an Al_2O_3/ZrO_2 laminates with smaller layer thicknesses.[4]

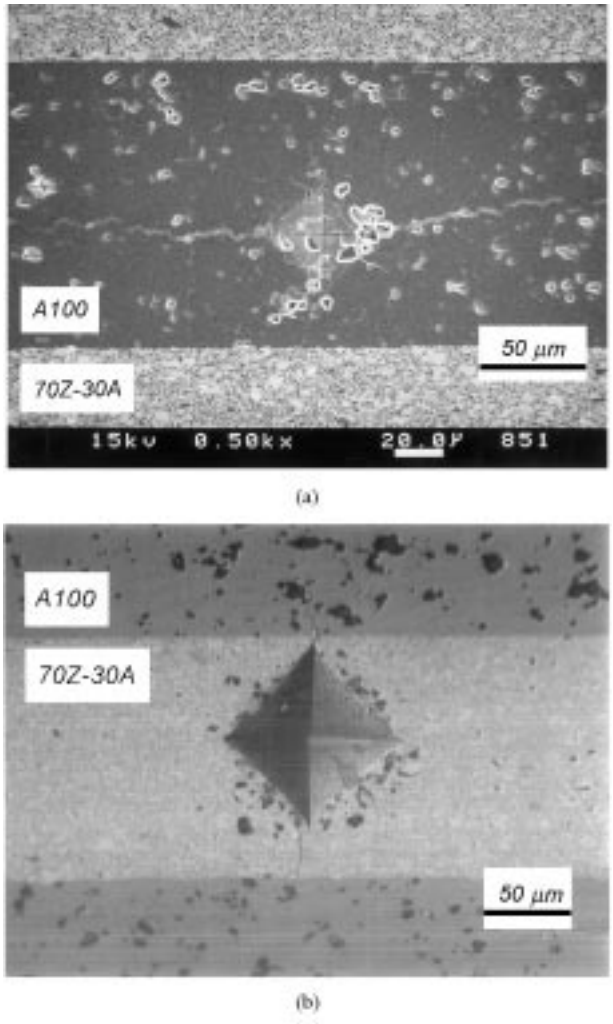

Fig. 3. Indentation placed on the cross-section of 1A–1Z. (a) A 19·6 N indent within the A100 layer; (b) a 49 N indent within the Z70–A30 layer.

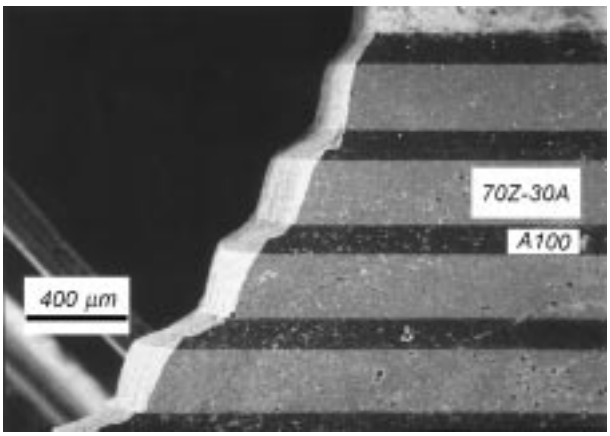

Fig. 4. SEM micrograph showing the tortuous crack path in an indentation-strength specimen.

3.3 Post-indentation strength

The post-indentation strengths are plotted against the indentation force on a logarithm scale in Fig. 5(a)–(c) for 1A-1Z, 1A-2Z and 0·5A–0·5Z, respectively. The best-fit curves of the function $\sigma_f = k_1 P^{-k_2}$, where σ_f is the post-indentation strength and k_1 and k_2 are constants, are also shown in the Fig. 5(a) and (c). The constant k_2 is included in the figures. It has been established[10] that if the fracture toughness of the material is a constant regardless of the crack size, or equivalently, the indentation force, the data points should fall on a straight line with a slope of $k_2 = 1/3$. It is

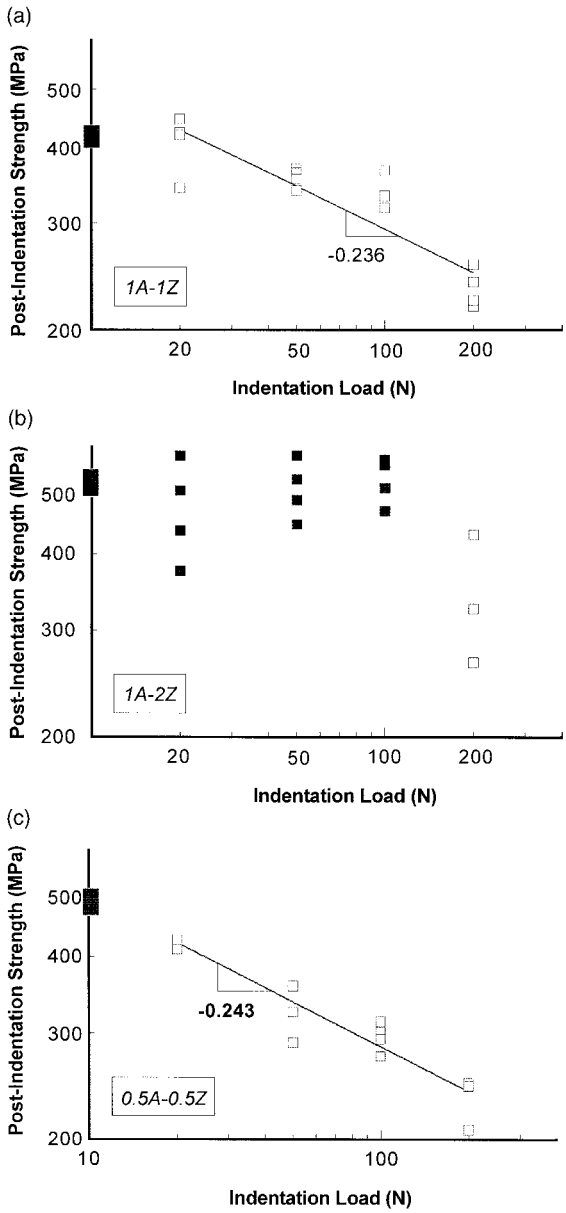

Fig. 5. Post-indentation strengths as a function of indentation force on a logarithm scale for hybrid laminates (a) 1A–1Z, (b) 1A–2Z and (c) 0·5A–0·5Z. The data points on the left represent the as-processed strength.

clear that the m values for the overall best-fit curves for 1A–1Z and 0·5A–0·5Z are less than 1/3, suggesting that the nominal toughness of these composites increases with the indentation force. Unlike the 1A–1Z and 0·5A–0·5Z laminates, the 1A–2Z specimens did not fail from the indents for indentation forces of 19·6, 49 and 98 N. Thus, the indentation force had no effect on the post-indentation strength at these indentation forces, i.e. the slope of the best-fit curve is zero. The 1A–2Z specimens at the 196 N indentation force did fail from the indent, and the post-indentation strength shows a significant decrease compared to lower indentation forces, as seen in Fig. 5(b).

It is known that the presence of surface residual compression leads to decreased sensitivity of the post-indentation strength versus indentation force. To determine if the observed deviation from the $-1/3$ slope in the laminates was indeed a result of the residual stress, the experimental results need to be compared with analytical predictions of the indentation strengths under the influence of the residual stress. In Appendix A, we show that, if the crack is contained well in the outer layer, the presence of the compressive stress increases the final failure surface stress by the amount equal to the magnitude of the residual stress:

$$\sigma_a + \sigma_r = \frac{3\chi P}{\Phi c_f^2} = \frac{3K_{Ic}^{4/3}}{4^{4/3}\chi^{1/3}} P^{-1/3} \tag{7}$$

where σ_a is the applied stress at failure, and c_f is the indentation crack size at failure. In theory, therefore, knowing the magnitude of the residual stress, one can predict the fracture stress as a function of the indentation force in the presence of σ_r.

However, since the two constituent layers of the laminates possess different moduli, the nominal strength plotted in Fig. 5, which assumes the bend bar is homogeneous, no longer represents the true stress at the A100 tensile surface upon failure. Since Al_2O_3 has a higher modulus than Z70, the true surface stress is always higher than the nominal stress. To calculate the true surface stress in the Al_2O_3, we use the classical laminate stress theory, in which biaxial layer stresses in a laminate with arbitrary layer sequences can be calculated. The detailed analysis is included in Appendix B. In the special case of alternating layers of equal thickness, it was shown in Appendix B that the ratio of the true maximum surface stress, σ_t, over the nominal stress, σ_n, is

$$\frac{\sigma_t}{\sigma_n} = \frac{E_1}{E_2 + (E_1 - E_2)\frac{(x+1)^2(2x-1)}{4x^3}} \tag{8}$$

in a symmetric laminate with $2x + 1$ layers. With measured values of E_1 and E_2, eqn (8) shows that, for a symmetric A100/Z70 laminate of 23 layers, $\sigma_t = 1{\cdot}2\sigma_n$. Substituting σ_t into σ_a in eqn (7), we obtain:

$$\sigma_n = \frac{\left(\frac{3K_{Ic}^{4/3}}{4^{4/3}\chi^{1/3}} P^{-1/3} - \sigma_r\right)}{1{\cdot}2} \tag{9}$$

Equation (9), which predicts the nominal strength as a function of the indentation force in the presence of the residual stress, is plotted in Fig. 6. Figure 6 also includes the experimentally obtained indentation strength data for laminate 1A–1Z. It is clear that there is good agreement between the analytical result and the experimental data. The agreement suggests that the observed increase of the nominal strength compared to monolithic Al_2O_3 can be explained solely by the presence of the residual surface compression.

3.4 Stable indentation crack growth prior to failure

It is well known that under externally applied stress the indentation cracks experience significant stable growth before catastrophic failure.[9,10] To determine the stable crack growth for the indented laminates in this study, surface trace lengths of the final crack length upon failure were recorded from the indents that did not fail in a multiple-indent strength specimen. The measured surface trace, c_f, for the 1A–1Z laminates is shown in Fig. 7(a), and the ratio of the surface trace of the final crack length over the initial crack length, c_f/c_0, is shown in Fig. 7(b) for the hybrid laminates as well as the monocomposition laminates. As seen in Fig. 7(b), the ratio is significant for the monocomposition laminates A100 and Z70–A30, but it is much smaller for the composite laminates, especially for 1A–2Z laminates.

In indentation theory,[9,10] the ratio of the final crack length to the initial crack length is equal to 2·52 for a residual stress free material. To consider

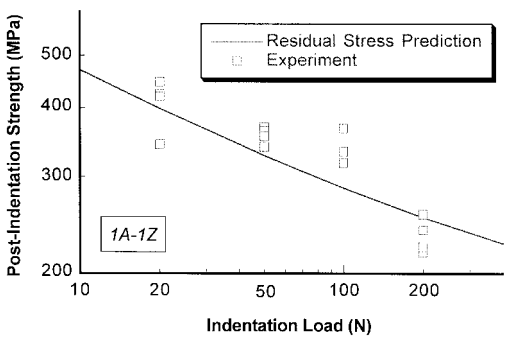

Fig. 6. Predicted nominal strength as a function of indentation force in the presence of the residual compression for 1A–1Z laminate. The data points are experimental results.

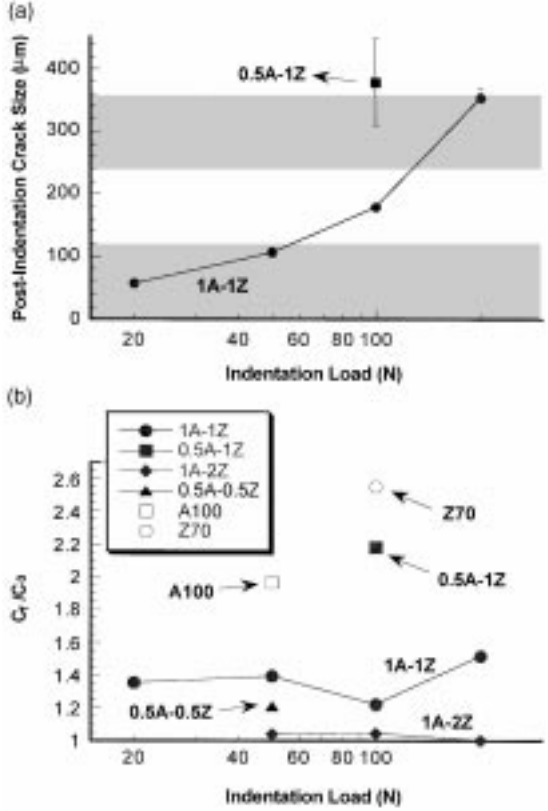

Fig. 7. (a) Surface trace of the final indentation crack length after failure for 1A–1Z; (b) The ratio of the surface trace of the final crack length over the initial crack length for the hybrid laminates and the monocomposition laminates.

the amount of indentation crack growth in the hybrid laminates, we need to examine the failure condition in terms of the stress intensity factors associated with the indent. The detailed analysis is given in Appendix A. In essence, unstable failure of the indentation crack ensues when the stress intensity factor equals the toughness of the layer and the derivative of the stress intensity factor with respect to the crack length equals to zero, viz.

$$K_1(c = c_f) = \chi P c_f^{-3/2} + \Phi\sigma_f c_f^{1/2} + \Phi\sigma_r c_f^{1/2} = K_{Ic}$$
$$\frac{dK_1}{dc}(c = c_f) = -\frac{3}{2}\chi P c_f^{-5/2} + \frac{1}{2}\Phi\sigma_f c_f^{-1/2} + \frac{1}{2}\Phi\sigma_r c_f^{-1/2} = 0 \quad (10)$$

Equation (10) holds only for cracks that are confined within the surface layer. By combining eqns (3) and (10), it can be shown that

$$c_f = 4^{2/3} c_0 \approx 2{\cdot}52 c_0 \quad (11)$$

This ratio is identical to the case where no residual stresses are present. Therefore, the final indentation crack length within a uniform residual stress field, in theory, is 2·52 times the initial indentation crack length in the *absence* of the residual stress field, c_0. In other words, in the case of residual compression where the indentation crack length, c_1, is smaller than c_0, the final indentation crack length under failure stress is *more than* 2·52 times the initial length c_1. In fact, by combining eqns (6) and (11), it can be shown $c_f \approx 3{\cdot}3c_1$ for a residual stress of −160 MPa.

This is in contradiction with the observation that the surface trace of the indentation crack for the hybrid laminates did not exhibit significant stable growth, as seen in Fig. 7(b). A reasonable explanation is that the majority of stable crack growth may have occurred in the thickness direction toward the Z70–A30 layer, while the surface trace of the indentation crack grew very little as a result of the compressive residual stress in the surface layer. Non-uniform crack growth of indentation cracks has been observed in an ion-exchanged glass,[17,18] where the indentation crack grew extensively towards the bulk while showing little growth on the compressive surface. It is to be noted that one exception to small surface trace growth was the data point marked '0·5A–1Z' in Fig. 7(b), which was obtained from a 1A–1Z sample with extensive surface polishing so that the surface A100 layer was almost reduced by half. For this specimen, the ratio c_f/c_0 is much larger than that for the other composite laminates for the indentation force of 98 N. This may be because the indentation crack has extended well into the 70Z–30A layer, which was in residual tension, and causing more crack extension of the surface trace.

Fractography of the indentation-strength specimens also appears to suggest the deviation from the semicircular crack during stable crack growth. Figure 8 shows a stereoscopic micrograph of the fracture surface of the 1A–1Z composite with a 196 N indent. While the crack front on such a polycrystalline fracture surface is difficult to define, the dark region in the vicinity of the original indent

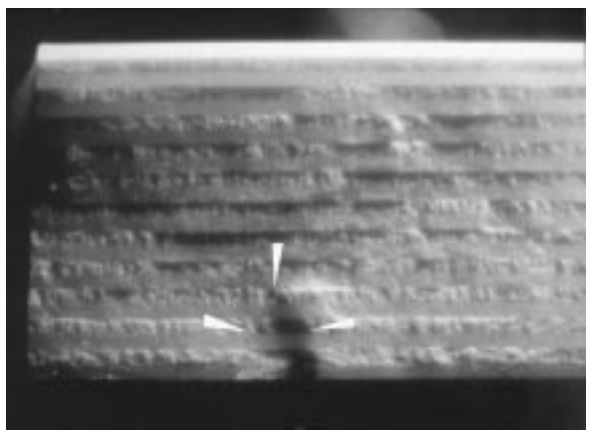

Fig. 8. Stereoscopic micrograph of the indentation crack on the fracture surface of 1A–1Z with a 196 N indent.

does seem to indicate the depth of the crack (a few layer thicknesses) is greater than its half surface trace.

4 Concluding remarks

Significant residual stresses due to the thermal expansion mismatch were found in the Al_2O_3/Ce–ZrO_2 laminated composites investigated in this study. The residual stresses were measured by evaluating the difference in indentation crack length with and without the residual stresses. The obtained residual stress values are in good agreement with the calculated residual stresses from the measured coefficients of thermal expansion for both layers. The observed increase in nominal toughness with increasing indentation force at low indentation forces (< 100 N) and a sudden decrease in post-indentation strength at the high indentation force (196 N) for the 1A–1Z can be explained as the effect of the compressive residual stress in the outer Al_2O_3 layer and also possibly the high toughness of the Z70–A30 layer. Larger layer thicknesses for the ZrO_2-containing layers, resulting in larger compressive residual stresses in the A100 layer, could lead to complete insensitivity of the failure strength to the indentation force as the failure no longer occurred at the indent, as seen in the 1A–2Z composites.

As the Z70–A30 layer has a higher toughness than the A100 layer, crack arrest may occur at the interface. However, crack arrest at the interface did not appear to be the mechanism dictating the final instability in the current laminates as the 1A–1Z and 0·5A–0·5Z show almost identical strengths. This is because the crack may reappear in the second or third A100 layers due to the low toughness of Al_2O_3, as suggested by the multiple layer damage within the Al_2O_3 layers at the 196 N load. To explore the possibility of multiple cracking and crack arrest solely in the surface layer by modulus and toughness modulation, as proposed in the work of Watkins and Green,[19,20] a much larger second layer thickness is needed, as well as a more drastic difference in layer modulus. Another possibility would be to place the second layer in residual compression.

It is evident that the Al_2O_3–ZrO_2 laminates are a promising composite design for enhancement of the mechanical behavior. Future effort should be focused on the interplay of the various potential strengthening and toughening mechanisms, including the surface residual compression, the difference in layer modulus and toughness, as well as the modification of the transformation zone of the Ce–ZrO_2 containing layers. In light of the requirements of the three mechanisms, the absolute layer thicknesses and the relative thickness ratios could be regulated to render optimum mechanical performance for this ceramic hybrid laminate.

References

1. Marshall, D. B., Ratto, J. J. and Lange, F. F., Enhanced fracture toughness in layered microcomposites of Ce–ZrO_2 and Al_2O_3. *J. Am. Ceram. Soc.*, 1991, **74**(12), 2979–2987.
2. Yttergren, R-M. F., Zeng, K. and Rowcliffe, D. J., Residual stress and crack propagation in laminated composites. In *Ceramic Transactions*, Vol. 46, ed., J. P. Singh and N. P Bansal. The American Ceramic Society, Columbus, OH, 1994.
3. Lakshminarayanan, R., Shetty, D. K. and Cutler, R. A., Toughening of layered ceramic composite with residual surface compression. *J. Am. Ceram. Soc.*, 1996, **79**(1), 79–87.
4. Prakash, O., Sarkar, P. and Nicholson, P. S., Crack deflection in ceramic/ceramic laminates with strong interfaces. *J. Am. Ceram. Soc.*, 1995, **78**(4), 1125–1127.
5. Wang, H. and Hu, X., Surface properties of ceramic laminates fabricated by die pressing. *J. Am. Ceram. Soc.*, 1996, **79**(2), 553–556.
6. Tandon, R. and Green, D. J., Crack stability and T-curves due to macroscopic residual compressive stress profiles. *J. Am. Ceram. Soc.*, 1991, **74**(8), 1981–1986.
7. Cai, P. Z., Green, D. J. and Messing, G. L., Constrained densification of Al_2O_3/ZrO_2 hybrid laminates, I. Experimental observations. *J. Am. Ceram. Soc.*, **80**(8), 1929–1939.
8. Cai, P. Z., Messing, G. L. and Green, D. J., Determination of the mechanical response of sintering compacts by cyclic loading dilatometry. *J. Am. Ceram. Soc.*, 1997, **80**(2), 445–452.
9. Anstis, G. R., Chantikul, P., Lawn, B. R. and Marshall, D. B., A critical evaluation of indentation techniques for measuring fracture toughness: I, Direct crack measurement, *J. Am. Ceram. Soc.*, 1981, **64**(9), 533–538.
10. Chantikul, P., Anstis, G. R., Lawn, B. R. and Marshall, D. B., A critical evaluation of indentation techniques for measuring fracture toughness: II, strength method. *J. Am. Ceram. Soc.*, 1981, **64**(9), 539–543.
11. Sathyamoorthy, R., Virkar, A. V. and Cutler, R. A., damage-resistant SiC–AlN layered composites with surface compressive stresses. *J. Am. Ceram. Soc.*, 1992, **75**(5), 1136–1141.
12. Hansen, J. J., Cutler, R. A., Shetty, D. K. and Virkar, A. V., Indentation fracture response and damage resistance of Al_2O_3–ZrO_2 composites strengthened by transformation induced residual stresses. *J. Am. Ceram. Soc.*, 1981, **71**(2), C–501–C-502.
13. Zeng, K. and Rowcliffe, D., Experimental measurement of residual stress field around a sharp indentation in glass. *J. Am. Ceram. Soc.*, 1994, **77**(2), 524–530.
14. Cai, P. Z., Green, D. J. and Messing, G. L., Constrained densification of Al_2O_3/ZrO_2 hybrid laminates, II. Viscoelastic stress. *J. Am. Ceram. Soc.*, 1997, **80**(8), 1940–1948.
15. Green, D. J. and Maloney, B. R., Influence of surface stress on indentation cracking. *J. Am. Ceram. Soc.*, 1986, **69**(3), 223–225.
16. Lawn, B. R. and Fuller Jr, E. R., Measurement of thin-layer surface stresses by indentation fracture. *J. Mater. Sci.*, 1984, **19**, 4061–4067.
17. Dwivedi, P. J., Crack-shape evolution during subcritical crack growth. Ph.D. thesis, The Pennsylvania State University, 1994.
18. Dwivedi, P. and Green, D. J., Indentation crack shape and its evolution in ion-exchanged glasses. In *Fractography Glasses and Ceramics III, Ceramic Transactions*, ed. J. R. Varner *et al.*, The American Chemical Society, Westerville, OH, 1996, pp. 473–490.

19. Watkins, T. R. and Green, D. J., Fracture behavior of CVD SiC–coated graphite: I, Experimental results. *J. Am. Ceram. Soc.*, 1993, **76**(12), 3066–3072.
20. Watkins, T. R. and Green, D. J., Fracture behavior of CVD SiC–coated graphite: II, Conditions for onset of multiple cracking. *J. Am. Ceram. Soc.*, 1994, **77**(3), 717–720.

Appendix A

Stress intensity factors associated with an indentation crack under both residual and applied stress

When an indentation crack is subjected to both residual stress and applied stress, the total stress intensity factor, ΣK_I, can be expressed as

$$\Sigma K_1 = K_i + K_r + K_a = \frac{\chi P}{c^{3/2}} + \Phi\sigma_r c^{1/2} + \Phi\sigma_a c^{1/2} \tag{A1}$$

where K_i, K_r and K_a represent the stress intensity factor associated with the residual stress around the indentation radial crack, the residual stress caused by thermal expansion mismatch and the externally applied stress, respectively. Failure occurs when the stress intensity factor reaches the toughness value, and the derivative of the stress intensity factor with respect to the crack size is zero. The two conditions are expressed as

$$K_1(c = c_f) = \chi P c_f^{-3/2} + \Phi\sigma_f c_f^{1/2} + \Phi\sigma_r c_f^{1/2} = K_{Ic} \tag{A2}$$

and

$$\frac{\mathrm{d}K_1}{\mathrm{d}c}(c = c_f) = -\frac{3}{2}\chi P c_f^{-5/2} + \frac{1}{2}\Phi\sigma_f c_f^{-1/2} + \frac{1}{2}\Phi\sigma_r c_f^{-1/2} = 0 \tag{A3}$$

respectively. In the meanwhile, a finite amount of crack growth also takes place. If the crack is embedded within the surface layer throughout the process, the amount of the crack growth can be determined as follows. The toughness is related to the as-indented crack length in the *absence* of the residual stress field, c_0, by

$$K_{Ic} = \chi \frac{P}{c_0^{3/2}} \tag{A4}$$

Multiplying eqn (A3) by c_f and equating it with eqn (10) gives:

$$c_f^{-3/2} = \frac{K_{Ic}}{4\chi P} \tag{A5}$$

Recognizing $c_0^{-3/2} = \frac{K_{Ic}}{\chi P}$, the relationship between c_f and c_0 is obtained:

$$c_f = 4^{2/3} c_0 \approx 2{\cdot}52 c_0 \tag{A6}$$

Equation (11) reveals that the final crack size is only dependent on c_0, regardless of the residual stress. It also follows from eqn (A3) that

$$\sigma_a + \sigma_r = \frac{3\chi P}{\Phi c_f^2} = \frac{3K_{Ic}^{4/3}}{4^{4/3}\chi^{1/3}} P^{-1/3} \tag{A7}$$

Equation (7) demonstrates that, if the toughness is not a function of crack size, the *sum* of the applied stress and the residual stress is proportional to the indentation force raised to the $-1/3$ power. The implication is that when the residual stress is compressive, the final failure stress will be less sensitive to the indentation force than the stress-free material. In other words, in the presence of a compressive residual stress field, the failure stress will deviate from the $-1/3$ slope on a logarithm plot versus the indentation force P.

Appendix B

Calculation of layer stress in a laminate with different layer moduli

For a homogeneous specimen loaded in four-point flexure, the maximum stress occurs at the tensile surface within the inner span, and the maximum stress is given as

$$\sigma = \frac{3P(l_o - l_i)}{2Bh^2} \tag{B1}$$

where P is the load at failure, B is the specimen width, h is the specimen thickness, and l_o and l_i are the outer span and the inner span, respectively. For a layered material with the layers having different elastic moduli, the above expression can only be considered a 'nominal' strength, and it no longer represents the true maximum surface stress upon failure. To calculate the maximum stress in four-point bending, one needs invoke the classical laminate stress analysis. In pure bending, the layer stress per unit thickness is related to the curvature of the beam, κ, by

$$\sigma_l = E\kappa z \tag{B2}$$

where z is the distance from the layer of interest to the neutral axis. For an alternately layered laminate with a sufficient number of layers, the neutral plane coincides with the half-thickness plane. The curvature is determined by the bending moment, M:

$$\kappa = \frac{M}{D} \tag{B3}$$

where

$$D = \frac{1}{3}\sum_k E_k\left(z_k^3 - z_{k-1}^3\right) \tag{B4}$$

and

$$M = \frac{P(l_o - l_i)}{4} \tag{B5}$$

In eqn (B4), the summation is over all the layers between the layer of interest and the neutral plane.

We shall derive a simple expression for a laminate consisting of alternately arranged component layers with a same thickness t. Without loss of generality, we assume the surface layer has a higher modulus, E_1, than the adjacent layer. In a symmetric laminate with $2n+1$ layers or an asymmetric laminate with $2n+1$ layers, where n is sufficiently large, the neutral plane can be assumed to coincide with the nth layer. In this case, eqn (B4) can be expressed as:

$$\begin{aligned} D &= \frac{1}{3}E_1 t^3\left[1^3 - 0^3 + 3^3 - 2^3 + \ldots + n^3 - (n-1)^3\right] \\ &+ \frac{1}{3}E_2 l^3\left[2^3 - 1^3 + 4^3 - 3^3 + \ldots + (n-1)^3 - (n-2)^3\right] \\ &= \frac{1}{3}(E_1 - E_2)t^3\left[1^3 - 2^3 + 3^3 - 4^3 + \ldots - (n-1)^3 + n^3\right] \\ &+ \frac{1}{3}E_2 n^3 t^3 = \frac{1}{3}(E_1 - E_2)t^3\sum_{i=1}^{n}(-1)^{i+1} i^3 + \frac{1}{3}E_2 n^3 t^3 \end{aligned} \tag{B6}$$

The summation in eqn (B6) can be simplified as

$$\begin{aligned} \sum_{i=1}^{n}(-1)^{i+1} i^3 &= \left(a^3 + 2^3 + \ldots + n^3\right) \\ &\quad - 2\left(2^3 + 4^3 + \ldots + (n-1)^3\right) \\ &= \sum_{i=1}^{n} i^3 - 16\sum_{j=1}^{\frac{n-1}{2}} j^3 \\ &= \frac{n^2(n+1)^2}{4} - 16\frac{\frac{(n-1)^2}{4}\left(\frac{n-1}{2}+1\right)^2}{4} \\ &= \frac{(n+1)^2(2n-1)}{4} \end{aligned} \tag{B7}$$

Equation (B7) is valid only when n is odd. When n is even, a similar expression can be readily derived. Substituting eqn (B7) into eqn (B6) and combining eqn (B2),(B3) and (B5), we arrive at the expression for the true maximum surface stress

$$\begin{aligned} \sigma_t &= \frac{E_1}{E_2 + (E_1 - E_2)\frac{(n+1)^2(2n-1)}{4n^3}} \cdot \frac{3P(l_o - l_i)}{2Bh^2} \\ &= \frac{E_1}{E_2 + (E_1 - E_2)\frac{(n+1)^2(2n-1)}{4n^3}} \cdot \sigma_n \end{aligned} \tag{B8}$$

In eqn (B8) σ_n is the nominal strength given by eqn (B1).